Article

Density Functional Theory Evaluation of a Photoinduced Intramolecular Aryl Ether Rearrangement

Péter Pál Fehér*

ACCESS | Metrics & More | Article Recommendations | Supporting Information

ABSTRACT: Recently, a new approach of converting (hetero)aryl ethers to C−C coupled products via a photoinduced intramolecular rearrangement has been reported. Although this reaction is photo-catalyst-free, it requires excitation in the ultraviolet (UV) range. To help refine this process, three different 2-(hetero)aryloxybenzaldehydes are selected from the available substrate scope in which the general mechanism based on experimental results is evaluated using density functional theory calculations. The reaction takes place in the triplet state after photoexcitation and includes three main steps: the addition of carbonyl carbon to the *ipso* carbon of the aryl ether followed by the C−O cleavage of the resulting spirocyclic intermediates and then the transfer of the formyl proton to afford 2-hydroxybenzophenone-type products. This agrees with the experiments, but the calculated pathways show considerable differences between the three substrates. Above all, either the first or the second step can be rate-determining but not the C−H activation. The important factor behind the differences is the spin-density rearrangement, which is mainly responsible for the barrier of the ether cleavage. Based on the obtained insights, the strategy to improve the ∼250 nm excitation has been briefly discussed, and promising molecules are proposed to improve the scope of this process.
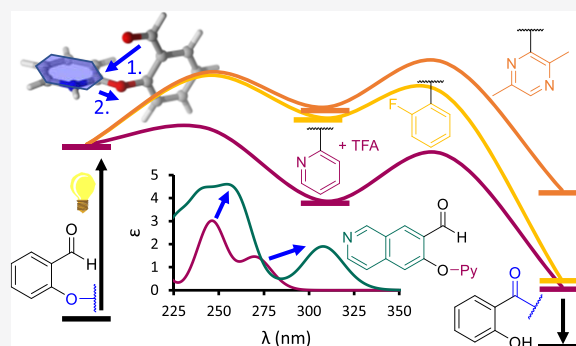
■ INTRODUCTION

Intramolecular rearrangements are perhaps the most attractive reaction steps in any organic synthesis because of their innate simplicity and atom efficiency. An existing example is the Smiles rearrangement, where an arene is transferred between two heteroatoms via intramolecular nucleophilic aromatic substitution.[1] Although such transformation of ethers is highly desirable because of their sustainability, the real impact to this field was the discovery of a way to produce C−C coupled products without activation on the migrating ring. In the Truce−Smiles rearrangement reaction (Scheme 1b), this is solved by generating a carbon nucleophile from the coupling group.[2] The original method involves deprotonation with strong bases like BuLi or KOtBu, but in recent contributions, several alternative approaches have been presented that exploit carbanion equivalents,[3] carbenes,[4] or aryl/acyl radicals.[5] Among these approaches, Zeng et al. present a remarkably convenient photoinduced reaction (Scheme 1a) that employs ultraviolet (UV) light without additional photocatalysts or the involvement of transition metals.[6] It has good functional group tolerance and works for both homo- and heteroarenes, and the authors also provide a brief experimental study about the mechanism. Given the large substrate scope, a deeper mechanistic understanding would provide ways for further improvement. For example, the authors propose a mechanism that is essentially the intramolecular variant of the one typically applied to the Minisci-type reactions (Scheme 1c).[7] It can cover

heterocyclic substrates in a straightforward manner, but it might require some alterations to work for homoaromatic compounds as they rearrange without external acids.

The mechanism assumes that the excitation of the 2-aryloxy salicylaldehyde substrate yields a carbonyl diradical, which behaves as a conventional carbon-based radical. It attacks the *ipso* carbon of the aryl ether, forming a spirocyclic intermediate that undergoes C−O bond cleavage and a final proton or hydrogen atom transfer to yield a benzophenone product. This is different from the typical radical-based mechanisms of Truce−Smiles reactions, which usually feature sulfonate esters to provide a driving force via SO₂ extrusion.[7b,8] In addition, Minisci-type reactions, by definition, involve C−H activation via the replacement of a hydrogen atom with a carbon-based radical next to a heteroatom in a conjugated ring. It has been established that in the case of pyridine, protonation not only prevents electrophilic attack on the basic nitrogen but also lowers the energy of the lowest unoccupied molecular orbital (LUMO) located on the aromatic ring.[9] This facilitates stronger
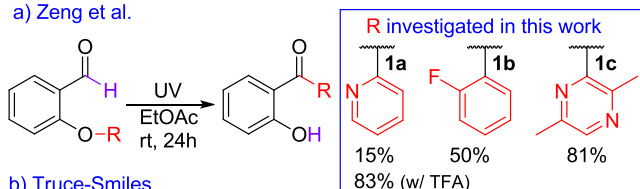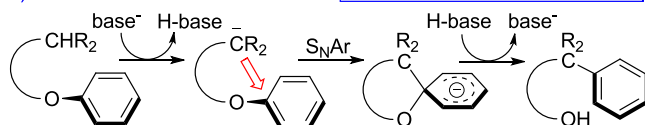
Scheme 1. Photoinduced Aryl Ether Rearrangement Reported by Zeng et al.[6] together with Mechanistic Scenarios That Are Typical of Truce−Smiles and Minisci Reactions[a]
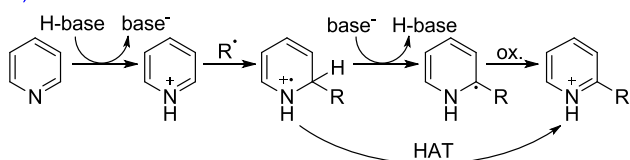

[a]The percentage yields (24 h) are taken from ref.[6]

interactions with nucleophilic (e.g., carbonyl) radicals. The benzene ring, however, has a higher-energy LUMO and is more susceptible to electrophilic attacks.[10] Indeed, similar photochemical reactions are actually called arylations because the radicals are generated from aryl halides.[11] In contrast, the salicylaldehyde ethers discussed here do not need to contain suitable leaving groups. It is therefore unclear whether such a mechanism can be assigned to ether C−O activation. The exploration of these issues sets the goal of this study to evaluate the mechanism proposed in ref.[6] using DFT calculations and explore whether it is applicable to ethers other than pyridyls. In addition, considering the excitation wavelength, visible-light-induced Minisci alkylation, arylation, and formylation have already been achieved, although with the use of added photocatalysts or exploiting the leaving groups.[12] Therefore, it would be appealing to observe how the 254 nm excitation in the presently discussed process can be improved upon. For this purpose, time-dependent density functional theory (TDDFT) and molecular orbital analysis are used to investigate the nature of the excitations and provide further insights.

COMPUTATIONAL DETAILS

All the calculations were carried out using the Gaussian16 software package.[13] The lowest energy triplet (ground-) states were calculated with unrestricted Kohn−Sham DFT, while the singlet excited states and spectra were obtained using TDDFT. The M06 functional was used for all calculations.[14] The geometries were optimized inside the solvent (ethyl acetate) cavity, as described by the implicit solvent model based on density (SMD).[15] The triple-ζ TZVP basis set was employed for structure optimization and frequency calculations.[16] The electronic energies were improved using the triple-ζ def2-TZVPP basis set.[17] Throughout this work, relative Gibbs free energies (ΔG) are reported for 25 °C and 1 atm external pressure. For the discussion of excited states, natural transition orbitals (NTOs) were calculated.[18]

RESULTS

The general mechanism proposed by Zeng et al.[6] is based on their control experiments carried out on the 2-(pyridin-2-yloxy)benzaldehyde substrate shown in Scheme 1a. First, the same molecule is used to evaluate the feasibility of this mechanism and to explore if other possible pathways are available. The results are then used to determine the key features responsible for providing the lowest possible energy barrier. Second, the other two ethers from Scheme 1a are discussed, focusing on the differences in their electronic structures relative to the pyridyl ether and how it affects their calculated mechanisms. The most apparent difference is the need for the protonation of pyridine because the other two substrates react without additives. Finally, the gained insights are used to provide a strategy for finding candidates that undergo isomerization more readily at higher wavelengths.

2-(Pyridin-2-yloxy)Benzaldehyde Substrates. It was established that the 2-(pyridin-2-yloxy)benzaldehyde molecule **1a** requires protonation to provide an optimal photoinduced isomerization yield. The neutral and the protonated species, however, have slightly different calculated UV absorption spectra (Figure 1). Two peaks appear at 247 and 280 nm for
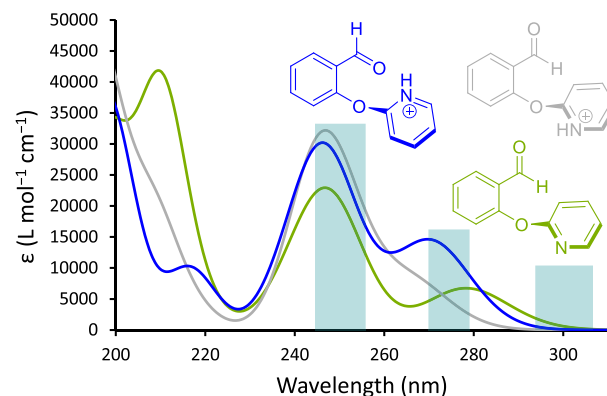

Figure 1. Calculated spectra of the neutral (green) and protonated (gray and blue) forms of **1a**. The gray structure is a minor conformer (ΔG = 2.0 kcal/mol) of the protonated molecule. The translucent rectangles indicate the positions and relative shapes of the bands around the peaks in the experimental[6] spectrum. The calculated spectra are obtained after summing the Gaussian functions that were applied to each excitation. The half width of the individual Gaussians is 0.2 eV.

the neutral molecule, respectively, while protonation shifts the absorption at 280 nm into the main band to appear as a shoulder peak at 267 nm. The main protonated conformer, however, has a carbonyl−aryl interaction which yields a more intensive and less-shifted lower energy band at 271 nm as well as additional excitations (Figure S1) above ~250 nm. The experimental absorption spectrum has similar features: a smaller band at 300 nm and a larger band at 250 nm with a shoulder at 270 nm.[6] Although not stated, if the spectrum was measured with or without added acid, the latter two features are reproduced almost exactly in the calculated spectra of the protonated isomers, while the 300 nm band can be assigned to the neutral molecule. It is to be noted that even the underestimation of the 300 nm peak by 20 nm yields a relative error of 7%, which is well within the typical accuracy of TDDFT.[19] These results indicate that the protonated **1a** absorbs light more readily; however, the 254 nm irradiation used in ref.[6] can excite the neutral molecules as well.

In a photochemical process, the light excites a ground state molecule with the closed-shell electronic configuration to its first excited singlet state (S1). The rapid depopulation via fluorescence or vibrational relaxation, however, only allows to overcome very small barriers on the S1 potential surface.[20] Therefore, it is conceptualized that photochemical reactions requiring additional thermal activation involve triplet states T1, which are reached from S1 via intersystem crossing (ISC).[21] This leads to the energy profile shown in Figure 2, which
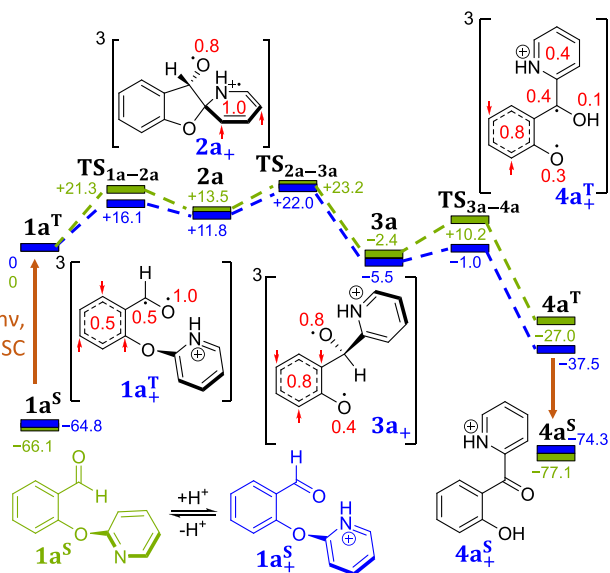

Figure 2. Energy profiles of the intramolecular rearrangement in the neutral (green) and protonated (blue) forms of **1a**. The energy values in colors matching the markers indicate the relative free energies and are denoted in units of kcal/mol. This convention is used throughout all the figures. The numbers in black correspond to the general structure numbering without regard to protonation. The numbers in red here and in the rest of the figures indicate the calculated Mulliken atomic spin populations at the corresponding atoms or summed over the phenyl groups with arrows pointing at the carbons with highest contribution. When describing pathways with protonated molecules, it is assumed that the concentration of neutral molecules is negligible in the system. This is supported by the strong acidity (pKa = 0.52) of trifluoroacetic acid (TFA).

indicates a thermally activated process for both the neutral and protonated **1a**, starting from their triplet reactant states.[22] According to the experimental mechanistic proposal and the Minisci model shown in Scheme 1c, a carbon-centered radical subunit triggers the substitution reaction shown in Scheme 1a. The spin density shown in Figure 2 for the protonated $\mathbf{1a^T}$ state indicates this phenomenon; carbonyl $n \rightarrow \pi^*$ excitation (Figures S2–3) yields a reactive carbon atom, which then attacks the *ipso* carbon of the aryl ether. The resulting spirocyclic intermediate **2a** is then cleaved at the ether side in a rate-determining step to yield a structure (**3a**) that resembles an alkoxy−phenoxy biradical. To obtain the final product, the hydrogen from benzylic carbon is transferred to the phenoxy oxygen in $\mathbf{TS_{3a-4a}}$. This is an ambimodal transition state as the phenol on the product side is not stable in the triplet state and either relaxes into the ground state (**4a^S**) or remains as a triplet alkyl alcohol (**4a^T**) through spontaneous H-transfer between the two oxygens.[23] The latter has an entirely planar structure, which is also indicated by its complete spin-density delocalization.

Evidently, this intermediate is expected to eventually relax to afford the final product, **4a^S**.

The comparison of the energy profiles of the neutral and protonated forms indicates that protonation yields a more favorable pathway, although the energy of the rate-determining $\mathbf{TS_{2a-3a}}$ differs by only 1.2 kcal/mol (22.0 vs 23.2 kcal/mol). The barrier of the radical attack at the *ipso* carbon ($\mathbf{TS_{1a-2a}}$), however, is affected by a considerably larger margin (5.2 kcal/mol). Therefore, the results are in line with a mechanism typical of Minisci reactions. The small difference between the two overall activation barriers, however, do not provide a convincing explanation for the observed experimental behavior (15% vs 83% yield). To explain this, a different approach is required.

As protonation is carried out in the presence of TFA in the experiments, the inclusion of this molecule into the model provides a more refined description of the reaction. This is shown in Figure 3, where the TFA molecule acts as a proton shuttle, transferring hydrogen from nitrogen in $\mathbf{2a_+}$ to yield a benzyl alcohol(**III**) in two steps. In **III**, the ether cleavage step to afford a phenoxy radical is almost barrierless. This intermediate **IV** undergoes intramolecular hydrogen atom transfer to restore the pyridinium ion, providing $\mathbf{3a_+}$ from which the reaction proceeds as shown in Figure 2. The difference between the two mechanisms lies in the rearrangement of the spin density prior to the C−O cleavage. By protonating the former carbonyl oxygen in **I**, a major part of the spin density is shifted to the phenyl ring (**II**, **III**), creating a biradical where the overall spin density is divided almost evenly between the two aromatic rings. The ether cleavage from **III** to obtain **IV** in this way requires no spin rearrangement, which is in contrast to the process depicted in Figure 2. Here, the entire spin density of the pyridinium radical moiety in $\mathbf{2a_+}$ is transferred to yield a phenoxy radical ($\mathbf{3a_+}$), indicating a process resembling oxidation that is depicted in Scheme 1b. In the TFA-assisted mechanism, the analogous process is the hydrogen atom transfer from the hydroxy group to the pyridine nitrogen ($\mathbf{IV} \rightarrow \mathbf{3a_+}$), which requires considerably less (4.9 kcal/mol) activation energy. It is to be noted that both the pathways can describe a Minisci-type reaction (Scheme 1b) as they start with radical attack and end with either oxidation or H-atom transfer. The common feature of the two approaches is that the rate-determining steps $\mathbf{2a_+} \rightarrow \mathbf{3a_+}$ and $\mathbf{I} \rightarrow \mathbf{II}$ involve the formation of a (pseudo-)phenoxy radical moiety, which is implied to be the key step of this reaction. Therefore, by involving TFA as a proton shuttle, the 22.0 kcal/mol barrier between $\mathbf{2a_+}$ and $\mathbf{3a_+}$ shown in Figure 2 becomes decreased to 16.4 kcal/mol, corresponding to a proton transfer step instead of ether cleavage. It is to be noted that the value 16.4 kcal/mol is very close to the barrier of the *ipso* addition (16.1 kcal/mol), preventing the unambiguous assignment of the rate-determining step.

The new intermediates (**II−IV**) introduced in Figure 3 indicate that the rearranging hydrogens yield a more favorable spirocyclic structure and a spin-density distribution more suitable for ether cleavage. Therefore, exploring other H-transfer scenarios could reveal additional favorable pathways. Considering an intramolecular process to obtain **III** from $\mathbf{2a_+}$ without TFA requires an energy of 22.7 kcal/mol, while the 1,2 H-rearrangement in $\mathbf{2a_+}$ between the C and O atoms of the former aldehyde group, has a barrier of 34.0 kcal/mol. Neither option is viable. The C−H activation of the aldehyde in $\mathbf{1a_+^T}$, however, yields entirely different energetics when the counterion (TFA) is included in the model. For comparison with the previous models, Figure 4 includes the mechanism where the salt of $\mathbf{2a_+}$
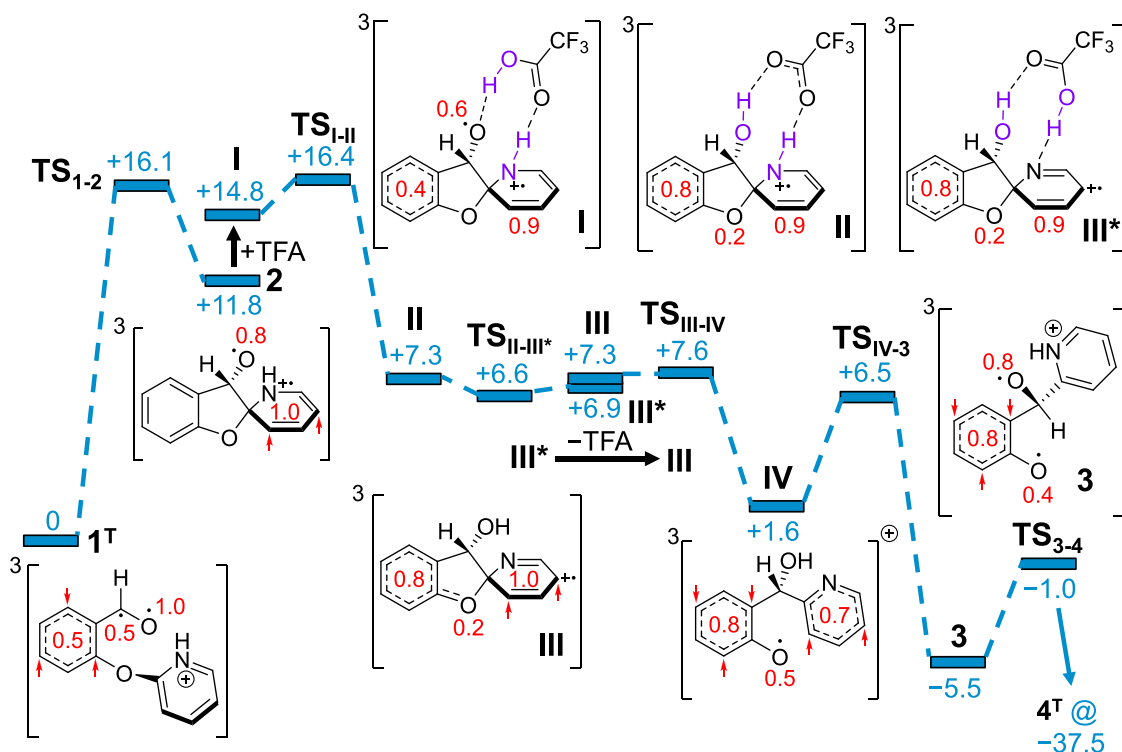
Figure 3. TFA-assisted isomerization of **1a**. The free energy of $TS_{II-III*}$ is below the corresponding minima because of the flat potential energy surface. The large energy changes to reach the $\mathbf{1a^T}$ and $\mathbf{4a}$ states, as seen in Figure 2, are not shown to increase clarity. The numbers in red correspond to Mulliken atomic spin populations, as described in the text of Figure 2.

forms and breaks. The corresponding 20.5 kcal/mol barrier is higher than those in the other cases as the acetate induces conformational changes unfavorable for the *ipso* addition. The deprotonation of the formyl group before cyclization, however, is a much more favorable step that requires only 4.4 kcal/mol activation energy. The resulting diradical **iii*** is different from **ii** as the spin populations on the carbonyl O (0.9 → 0.5) and C (0.5 → 0.9) atoms are flipped. The almost one equivalent of an unpaired electron opens the way for an almost barrierless spirocycle (**v**) formation and a successive proton transfer from TFA to yield benzyl alcohol **vi**. The rate-determining step is the following C−O cleavage (TS_{vi-vii}), providing a very low barrier of 12.5 kcal/mol. The difference between TS_{vi-vii} and the analogous transition states (TSs) in the mechanisms discussed so far is that among the preceding intermediates (**vi**, **2a**$_+$, and **III**), **vi** exhibits continuously delocalized spin-density distribution between the two aromatic rings because of the linking sp^2 carbon in the benzyl position. Although this situation is the least favorable for C−O cleavage,[24] the overall 12.5 kcal/mol barrier provided here is the lowest among the three pathways. Therefore, facilitating the *ipso* addition and the formation of a more stable spirocyclic intermediate are more important than the spin rearrangement for C−O cleavage.

Figure 4 also presents a different pathway where instead of undergoing ether cleavage, intermediate **v** relaxes to the ground state (**v**^{S}). The change in geometry between the two states is relatively small, but the bond between the *ipso* carbon and the ether oxygen is increased from 1.41 to 1.53 Å. This implies a more facile C−O cleavage. Indeed, it only consumes an energy of 2.1 kcal/mol. Therefore, the new pathway has an overall barrier of only 4.4 kcal/mol, corresponding to the rate-determining triplet C−H activation. Although the experimental kinetic isotope effect (KIE) result indicates no rate-determining

C−H activation,[6] this process is sufficiently fast to assume that it cannot be measured properly. It is to be noted that the triplet to singlet transition is already slower than the triplet C−O cleavage through TS_{vi-vii} as the barrier of 12.5 kcal/mol corresponds to a half-life of 1.64×10^{-4} s, as determined using the transition-state theory.[25] This indicates an at least one order of magnitude faster process compared to the T1 → S0 relaxation, which is typically in the 10^{-3} to 100 s range.[26] For comparison, $TS_{ii-iii*}$ at 4.4 kcal/mol yields a half-life of 1.87×10^{-10} s, while $TS_{2a\,+\,-3a+}$ and TS_{I-II} provide 1.52×10^3 s and 1.19×10^1 s, respectively.

Investigating the Mechanism of Other Substrates. The 2-(2-fluorophenoxy)benzaldehyde molecule **1b** is perhaps the simplest molecule investigated by Zeng et al.[6] There is no possibility of protonation; however, it still undergoes isomerization. Figure 5 indicates that TS_{1b-2b}, corresponding to the *ipso* attack in **1b**, is located between the neutral and protonated TS_{1a-2a} in energy, while the resulting spirocyclic intermediate **2b** is the most stable among the three. The lower energy of **2b** shifts the rest of the energy profile down from the level of **2b**, causing the initial *ipso* addition to become the rate-determining step of the mechanism. It is therefore apparent that adding the acid to facilitate C−O cleavage in **2b** according to the model in Figure 3 would not have any effect on the reaction rate as this step occurs after the rate-determining step. Thus, the barrier of isomerization is 18.3 kcal/mol, which is slightly higher than 16.4 kcal/mol calculated for the protonated pyridyl ether with a TFA proton shuttle. It is to be noted that as no sites of protonation are available for this molecule, neither models with TFA can be used here. Therefore, the only other investigated mechanistic scenario is the relaxation of the intermediates to the ground state. The relaxation of the spirocyclic **2** intermediates yields the initial **1**^{S} state for all the three ethers shown in Figure 5, while intermediates **3a**, **3a**$_+$, and **3b** provide epoxides (Figure S4). The
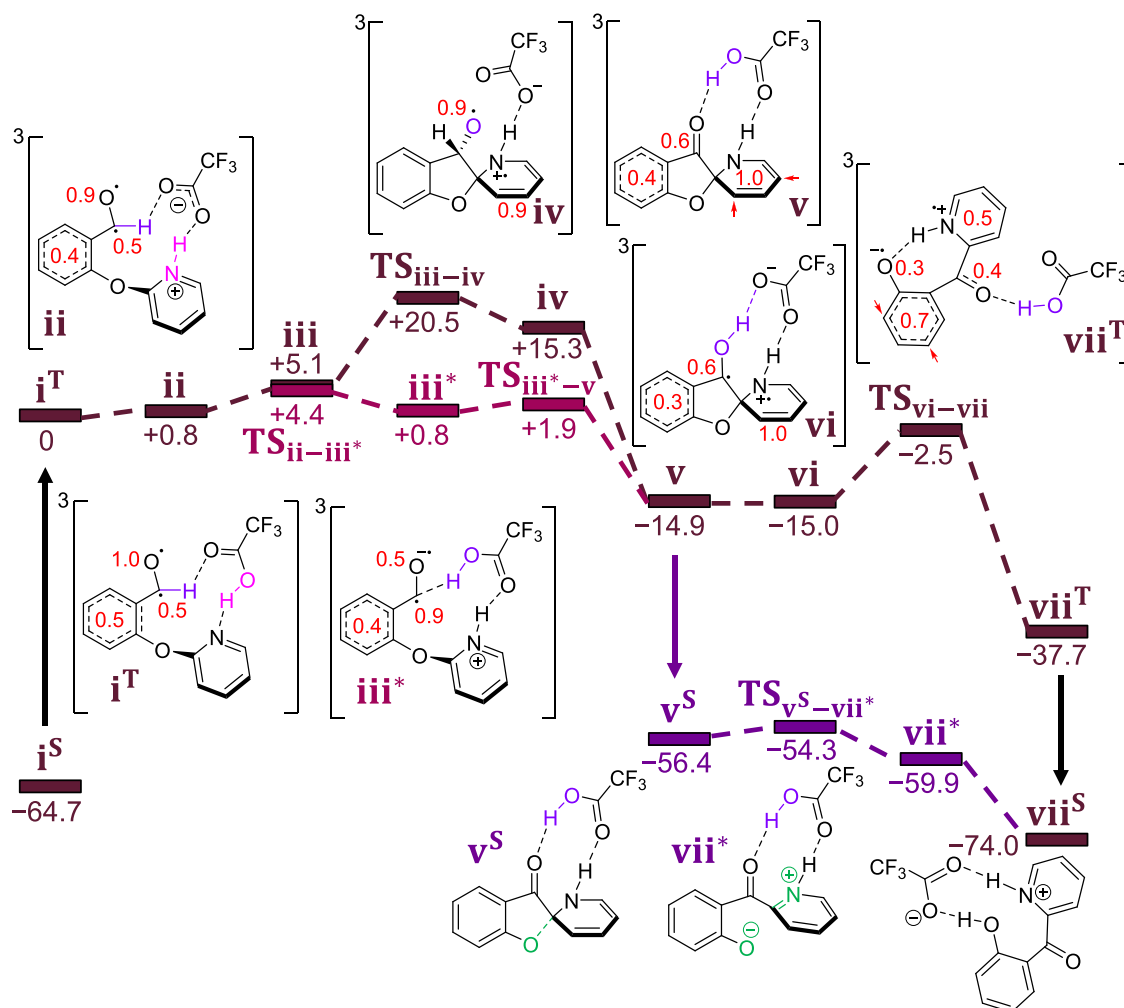
Figure 4. Three calculated pathways for the isomerization of the pyridinium ether salt **i**. Low-energy internal rotations and proton-transfer steps are not shown for a clear representation of the important features of the mechanisms.
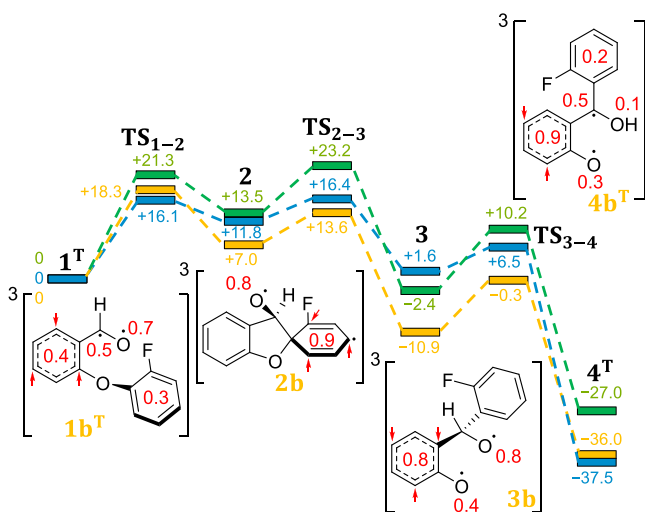

Figure 5. Energy profiles of the rearrangement of pyridyl (green: neutral, blue: protonated) and fluorophenyl (yellow) ethers. The structure indicators in black correspond to the general structure numbering without regard to the type of the migrating aromatic ring and its protonation state.

latter option, however, should not be relevant as **3** only appears after the rate-determining step in all the three energy profiles, while the former is simply the reverse process of the *ipso* addition that restarts the reaction.

The third type of aryl ether investigated in the present work contains a pyrazine ring. The experimental results indicated no need for activation via protonation, which makes the 2-((3,6-dimethylpyrazin-2-yl)oxy)benzaldehyde molecule **1c** similar to **1b** instead of **1a**. This points to an already electron-deficient ring, which agrees with the reduced basicity (pKa 0.6 for the protonated pyrazine and pKa 5.20 for the pyridinium cation) of pyrazine compared to pyridine. Indeed, Figure 6 shows that the *ipso* addition step of the neutral molecule has a barrier height similar to those of the other two ethers. The protonated form has significantly inferior energetics which is likely due to the different spin-density distribution of the **1**[T] states (Figure 6). In this regard, the neutral molecule is identical to the other ethers, while the two protonated isomers have almost all the spin density situated on the pyrazine ring. This means that there is no carbonyl radical available to initiate the reaction. The spirocyclic intermediates **2c**[1NH] and **2c**[4NH], however, can still form, although at a higher energy and through a considerably higher barrier. In case of the neutral molecule, the two diastereomers (**2c** and **2c***) of intermediate **2** provide different energetics for the two main reaction steps. The one with the less favored 19.1 kcal/mol
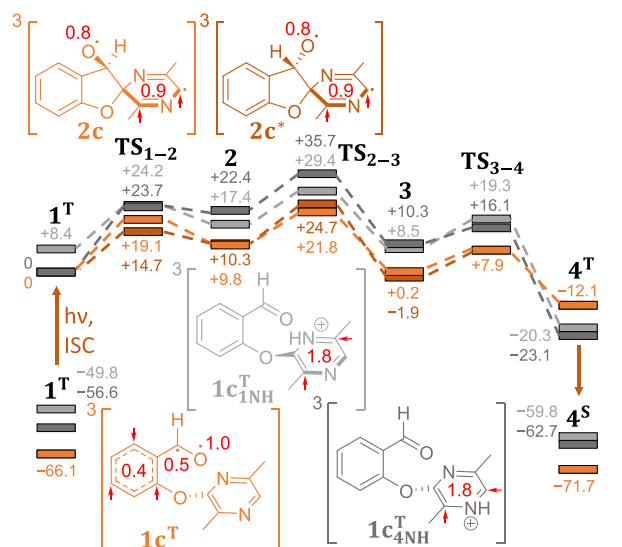
Figure 6. Energy profiles of the rearrangement of the pyrazine ether. The 1- and 4-protonated forms are shown in two shades of gray. The neutral molecule is presented in two shades of orange, representing the difference between the formation and cleavage of the two possible spirocyclic (**2c** and **2c***) diastereomers.

addition step yields a lower energy pathway, as the rate-determining ether cleavage TS_{2c-3c} lies lower at 21.8 kcal/mol.

As the basicity of the nitrogen atoms in the spirocyclic intermediates can be different from the initial state, additional hydrogen transfer steps were also investigated (Scheme S1). One of them involves hydrogen abstraction from the benzyl carbon by the nearest nitrogen in **2c** at +9.8 kcal/mol. As the corresponding TS_{2c-s1} is located at +23.7 kcal/mol, such a pathway cannot be competitive. The same is true for 1,2-hydrogen migration between the C and O atoms of the former carbonyl group, which has an even higher barrier (30.7 and 30.9 kcal/mol through TS_{2c-s2} and TS_{2c*-s2}). The H-transfer to the ether oxygen was also investigated, but potential energy scans revealed an uphill process reaching very high energies without a well-defined TS. These pathways would also provide rate-determining C−H activation, which is ruled out using experiments. It must be noted, however, that such evidence only exists for pyridyl ether.

Applying Structural Modifications to Improve Absorption. The ∼250 nm excitation used for the investigated aryl ethers presents a severe limitation for this reaction. Therefore, several molecules are evaluated here to find a way to increase the absorption wavelength as much as possible. A value of 300 nm would already be a significant improvement as most solvents, like ethyl acetate employed in this reaction, exhibit significant absorbance starting at 250 nm. Also, it must be noted that even among the three molecules investigated above, **1b** already has a predicted absorption band at 297 nm (Figure S5). This indicates that a part of the substrate scope reported in ref.[6] could have been successfully excited at higher wavelengths.

The investigation presented here involves the protonated **1a**. The NTO analysis in Figure S2 reveals that the carbonyl $n \rightarrow \pi^*$ excitation is a dark state (zero oscillator strength) located at 332 nm. As the intensive band at around 250 nm is composed of excitations with a pronounced $\pi \rightarrow \pi^*$ character, the alteration of the conjugated ring-based transitions should be the goal of structure modifications. The presence of such transitions of the migrating ring is not necessarily an undesirable feature (Figure

S2); however, the protonated pyrazine (Figure 5) and quinoline[6] ethers indicate that the modification of this ring can yield a nonreactive triplet state. This suggests a strategy to target the salicylaldehyde part of the reactive substrates because in this way, the carbonyl $n \rightarrow \pi^*$ excitation character of both the lowest singlet (S1) excited state and the lowest triplet (T1) state can be retained. The local $\pi \rightarrow \pi^*$ excitation of a modified phenyl ring can readily provide a relaxed $n \rightarrow \pi^*$ state of the carbonyl group because both are a part of the same conjugated system. One way to achieve this is through ring substituents. However, this strategy was not successful with the Me or NO_2 groups (Figure S6−7). Furthermore, expanding the conjugated system with condensed rings or phenyl substituents offers a more pronounced effect on the absorption spectra. Figure 7
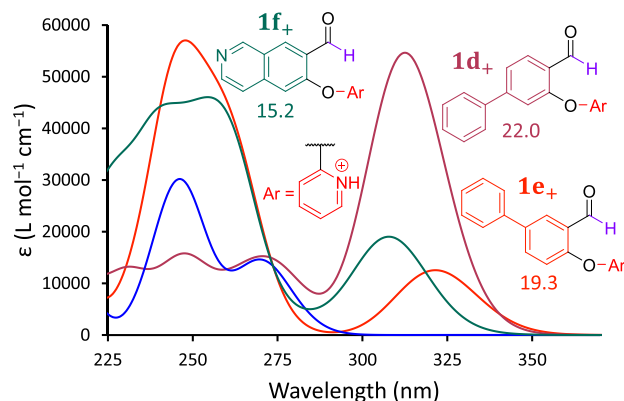

Figure 7. Three most successful structure modification attempts to shift the absorption above 300 nm. The numbers below the structures indicate the *ipso* addition barriers in kcal/mol. The blue spectrum corresponds to the protonated 2-(pyridin-2-yloxy)benzaldehyde (**1a**$_+$) molecule.

presents the substrate candidates for which the spirocyclic intermediate **2** is obtained through a barrier comparable to the **1a-c** molecules. They all exhibit a lowest energy dark state near 330 nm (Figure S8) with the carbonyl $n \rightarrow \pi^*$ character, which is similar to the unmodified molecule. Figures S9−11 show the spectra of all the probed molecules. The protonated 3-(pyridin-2-yloxy)-[1,1′-biphenyl]-4-carbaldehyde (**1d**) and 4-(pyridin-2-yloxy)-[1,1′-biphenyl]-3-carbaldehyde (**1e**) molecules shown in Figure 7 bear phenyl substituents in the *para* and *meta* positions relative to the carbonyl group with significant absorptions at 321 and 312 nm, respectively. The third, 2-((3,6-dimethylpyrazin-2-yl)oxy)benzaldehyde (**1f**) molecule absorbs at the lowest 308 nm wavelength among the three. However, it also has the lowest 15.2 kcal/mol barrier for the *ipso* addition, whereas the other two molecules exhibit values near 20 kcal/mol.[27] The largest 22.0 kcal/mol barrier of the protonated **1d** corresponds to a half-life of 1.52×10^3 s. Although this indicates a process slower than the T1 → S0 relaxation, the considerably higher molar absorption suggests that the triplet state can be populated more efficiently, leaving more chance for thermal activation to occur. Overall, these results show that simple structural modifications can readily improve the applicability of the intramolecular rearrangement process.

■ **CONCLUSIONS**

In this work, a photoinduced intramolecular (hetero)aryl ether rearrangement has been investigated using DFT calculations. The reaction was recently discovered by Zeng et al.,[6] who also

2711

provided a plausible mechanism based on their experimental results. The diversity of the salicylaldehyde ether substrates and the very low (254 nm) excitation wavelength, however, warranted a more comprehensive investigation to help refine the process. The computational results, overall, support the experiments and provide a general mechanism with five steps: the formation of a triplet carbonyl diradical-like state via UV excitation followed by a C−C *ipso* addition to yield a spirocyclic intermediate which undergoes C−O cleavage in an overall substitution reaction. The final product is obtained after H-transfer and relaxation of the ground state. The three main triplet-state reaction steps exhibit features of mechanisms typical of both the Truce−Smiles and Minisci reactions. These pathways feature activation barriers in the range of 16−22 kcal/mol for the three chosen substrates, with the rate-determining steps being either the *ipso* addition or the C−O cleavage. In case of 2-(pyridin-2-yloxy)benzaldehyde, the role of adding an external acid (TFA) is explained by the availability of a different pathway which starts with protonating the pyridine and deprotonating the aldehyde group using TFA to aid the *ipso* addition. In this manner, the energy barrier drops to a low level of 12.5 kcal/mol. The analysis also reveals that the TFA-induced tautomerization steps are responsible for reducing the electron density of the heterocycle and the rearrangement of the spin density. The former plays a role in the *ipso* addition step while the latter facilitates the rate-determining C−O cleavage.

Based on the results of the mechanistic investigation, a strategy for finding additional substrates that undergo the isomerization process more readily is proposed. For this purpose, several molecules were derived from the 2-(pyridin-2-yloxy)benzaldehyde molecule. The evaluation was based on the lowest energy absorption wavelength and the barrier of the *ipso* addition step. For the former, a value of 300 nm offers a reasonable improvement and can easily be achieved. As the goal is the excitation of the carbonyl group, the extension of conjugation at the salicylaldehyde half of the molecule presents a viable approach. This can be performed by adding condensed rings or forming a biphenyl, which are the commonly used building blocks of dyes or photocatalyst molecules. Considering the barrier of the *ipso* addition as well, the 2-quinoline backbone is especially promising with a barrier of 15.2 kcal/mol and predicted absorption at 308 nm. There is, however, no simple relation between the characteristic excitation and the barrier of addition shown by the investigated molecules. Nevertheless, the results indicate that the reaction scope reported by Zeng et al.[6] can be improved even further, and the potential substrates can be identified with relatively simple calculations.

ASSOCIATED CONTENT

Supporting Information

The Supporting Information is available free of charge at https://pubs.acs.org/doi/10.1021/acs.joc.0c02706.

The most stable conformations of the protonated and neutral **1a**; natural transition orbitals of the (protonated) **1a**; the structure of the epoxide intermediates; inferior reaction steps for the mechanism of **1c** shown in Figure 5; calculated absorption spectra of the three salicylaldehyde ethers; calculated absorption spectra of the Me and NO$_2$-substituted **1a$_+$**; NTOs of the first excited state of the molecules shown in Figure 7; calculated absorption spectra of the modified salicylaldehyde ethers; the *ipso*

attack step for **1a** in the S1 state; and coordinates and energies of the computed structures (PDF).

Cartesian coordinates (XYZ)

AUTHOR INFORMATION

Corresponding Author

Péter Pál Fehér − *Research Centre for Natural Sciences, H-1117 Budapest, Hungary;* orcid.org/0000-0002-6927-4523; Email: feher.peter@ttk.hu

Complete contact information is available at:
https://pubs.acs.org/10.1021/acs.joc.0c02706

Notes

The author declares no competing financial interest.

REFERENCES

(1) (a) Levy, A. A.; Rains, H. C.; Smiles, S. CCCCLII.—The Rearrangement of Hydroxy-Sulphones. Part I. *J. Chem. Soc.* **1931**, *0*, 3264−3269. (b) Bunnett, J. F.; Zahler, R. E. Aromatic Nucleophilic Substitution Reactions. *Chem. Rev.* **1951**, *49*, 273−412. (c) Holden, C. M.; Greaney, M. F. Modern Aspects of the Smiles Rearrangement. *Chem. − Eur. J.* **2017**, *23*, 8992−9008.

(2) (a) Truce, W. E.; Ray, W. J., Jr.; Norman, O. L.; Eickemeyer, D. B. Rearrangements of Aryl Sulfones. I. The Metalation and Rearrangement of Mesityl Phenyl Sulfone1. *J. Am. Chem. Soc.* **1958**, *80*, 3625−3629. (b) Snape, T. J. A Truce on the Smiles Rearrangement: Revisiting an Old Reaction—the Truce−Smiles Rearrangement. *Chem. Soc. Rev.* **2008**, *37*, 2452. (c) Henderson, A. R. P.; Kosowan, J. R.; Wood, T. E. The Truce−Smiles Rearrangement and Related Reactions: A Review. *Can. J. Chem.* **2017**, *95*, 483−504.

(3) Rao, H.; Li, C.-J. Rearrangement of 2-Aryloxybenzaldehydes to 2-Hydroxybenzophenones by Rhodium-Catalyzed Cleavage of Aryloxy C−O Bonds. *Angew. Chem., Int. Ed.* **2011**, *50*, 8936−8939.

(4) Janssen-Müller, D.; Singha, S.; Lied, F.; Gottschalk, K.; Glorius, F. NHC-Organocatalyzed CAr Bond Cleavage: Mild Access to 2-Hydroxybenzophenones. *Angew. Chem., Int. Ed.* **2017**, *56*, 6276−6279.

(5) (a) Li, J.; Liu, Z.; Wu, S.; Chen, Y. Acyl Radical Smiles Rearrangement To Construct Hydroxybenzophenones by Photoredox Catalysis. *Org. Lett.* **2019**, *21*, 2077−2080. (b) Abrams, R.; Clayden, J. Photocatalytic Difunctionalization of Vinyl Ureas by Radical Addition Polar Truce−Smiles Rearrangement Cascades. *Angew. Chem., Int. Ed.* **2020**, *59*, 11600−11606.

(6) Dou, Q.; Li, C.-J.; Zeng, H. Photoinduced Transition-Metal- and External-Photosensitizer-Free Intramolecular Aryl Rearrangement via C(Ar)−O Bond Cleavage. *Chem. Sci.* **2020**, *11*, 5740−5744.

(7) (a) Minisci, F.; Galli, R.; Cecere, M.; Malatesta, V.; Caronna, T. Nucleophilic Character of Alkyl Radicals: New Syntheses by Alkyl Radicals Generated in Redox Processes. *Tetrahedron Lett.* **1968**, *9*, 5609−5612. (b) Proctor, R. S. J.; Phipps, R. J. Recent Advances in Minisci-Type Reactions. *Angew. Chem., Int. Ed.* **2019**, *58*, 13666−13699.

(8) (a) Rashid, S. O.; Almadhhi, S. S.; Berrisford, D. J.; Raftery, J.; Vitorica-Yrezabal, I.; Whitehead, G.; Quayle, P. Radical Truce-Smiles Reactions on an Isoxazole Template: Scope and Limitations. *Tetrahedron* **2019**, *75*, 2413−2430. (b) Allart-Simon, I.; Gérard, S.; Sapi, J. Radical Smiles Rearrangement: An Update. *Molecules* **2016**, *21*, 878. (c) Barlow, H. L.; Rabet, P. T. G.; Durie, A.; Evans, T.; Greaney, M. F. Arylation Using Sulfonamides: Phenylacetamide Synthesis through Tandem Acylation−Smiles Rearrangement. *Org. Lett.* **2019**, *21*, 9033−9035.

(9) Tauber, J.; Imbri, D.; Opatz, T. Radical Addition to Iminium Ions and Cationic Heterocycles. *Molecules* **2014**, *19*, 16190−16222.

(10) (a) Rohrbach, S.; Smith, A. J.; Pang, J. H.; Poole, D. L.; Tuttle, T.; Chiba, S.; Murphy, J. A. Concerted Nucleophilic Aromatic Substitution Reactions. *Angew. Chem., Int. Ed.* **2019**, *58*, 16368−16388. (b) Smith, M.; March, J. *March's advanced organic chemistry: reactions, mechanisms, and structure*; Wiley-Interscience: Hoboken, N.J, 2007.

(11) (a) Ghosh, I.; Marzo, L.; Das, A.; Shaikh, R.; König, B. Visible Light Mediated Photoredox Catalytic Arylation Reactions. *Acc. Chem. Res.* **2016**, *49*, 1566−1577. (b) Twilton, J.; Le, C.; Zhang, P.; Shaw, M. H.; Evans, R. W.; MacMillan, D. W. C. The Merger of Transition Metal and Photocatalysis. *Nat. Rev. Chem.* **2017**, *1*, No. 0052.

(12) (a) Dong, J.; Lyu, X.; Wang, Z.; Wang, X.; Song, H.; Liu, Y.; Wang, Q. Visible-Light-Mediated Minisci C−H Alkylation of Heteroarenes with Unactivated Alkyl Halides Using O2 as an Oxidant. *Chem. Sci.* **2019**, *10*, 976−982. (b) Dong, J.; Wang, X.; Song, H.; Liu, Y.; Wang, Q. Photoredox-Catalyzed Redox-Neutral Minisci C−H Formylation of N -Heteroarenes. *Adv. Synth. Catal.* **2020**, *362*, 2155−2159. (c) Xue, D.; Jia, Z.-H.; Zhao, C.-J.; Zhang, Y.-Y.; Wang, C.; Xiao, J. Direct Arylation of N-Heteroarenes with Aryldiazonium Salts by Photoredox Catalysis in Water. *Chem. − Eur. J.* **2014**, *20*, 2960−2965. (d) Bieszczad, B.; Perego, L. A.; Melchiorre, P. Photochemical C−H Hydroxyalkylation of Quinolines and Isoquinolines. *Angew. Chem., Int. Ed.* **2019**, *58*, 16878−16883.

(13) Frisch, M. J.; Trucks, G. W.; Schlegel, H. B.; Scuseria, G. E.; Robb, M. A.; Cheeseman, J. R.; Scalmani, G.; Barone, V.; Petersson, G. A.; Nakatsuji, H.; Li, X.; Caricato, M.; Marenich, A. V.; Bloino, J.; Janesko, B. G.; Gomperts, R.; Mennucci, B.; Hratchian, H. P.; Ortiz, J. V.; Izmaylov, A. F.; Sonnenberg, J. L.; Williams-Young, D.; Ding, F.; Lipparini, F.; Egidi, F.; Goings, J.; Peng, B.; Petrone, A.; Henderson, T.; Ranasinghe, D.; Zakrzewski, V. G.; Gao, J.; Rega, N.; Zheng, G.; Liang, W.; Hada, M.; Ehara, M.; Toyota, K.; Fukuda, R.; Hasegawa, J.; Ishida, M.; Nakajima, T.; Honda, Y.; Kitao, O.; Nakai, H.; Vreven, T.; Throssell, K.; Montgomery, J. A., Jr.; Peralta, J. E.; Ogliaro, F.; Bearpark, M. J.; Heyd, J. J.; Brothers, E. N.; Kudin, K. N.; Staroverov, V. N.; Keith, T. A.; Kobayashi, R.; Normand, J.; Raghavachari, K.; Rendell, A. P.; Burant, J. C.; Iyengar, S. S.; Tomasi, J.; Cossi, M.; Millam, J. M.; Klene, M.; Adamo, C.; Cammi, R.; Ochterski, J. W.; Martin, R. L.; Morokuma, K.; Farkas, O.; Foresman, J. B.; Fox, D. J. Gaussian 16, Revision A.03, Gaussian, Inc., Wallingford CT, 2016.

(14) Zhao, Y.; Truhlar, D. G. The M06 Suite of Density Functionals for Main Group Thermochemistry, Thermochemical Kinetics, Non-covalent Interactions, Excited States, and Transition Elements: Two New Functionals and Systematic Testing of Four M06-Class Functionals and 12 Other Functionals. *Theor. Chem. Acc.* **2007**, *120*, 215−241.

(15) Marenich, A. V.; Cramer, C. J.; Truhlar, D. G. Universal Solvation Model Based on Solute Electron Density and on a Continuum Model of the Solvent Defined by the Bulk Dielectric Constant and Atomic Surface Tensions. *J. Phys. Chem. B* **2009**, *113*, 6378−6396.

(16) (a) Ehlers, A. W.; Böhme, M.; Dapprich, S.; Gobbi, A.; Höllwarth, A.; Jonas, V.; Köhler, K. F.; Stegmann, R.; Veldkamp, A.; Frenking, G. A set of f-polarization functions for pseudo-potential basis sets of the transition metals Sc-Cu, Y-Ag and La-Au. *Chem. Phys. Lett.* **1993**, *208*, 111−114. (b) Hay, P.; Jeffrey, W.; Willard, R. Ab initio effective core potentials for molecular calculations. Potentials for K to Au including the outermost core orbitals. *J. Chem. Phys.* **1985**, *82*, 299−310. (c) Roy, L. E.; Hay, P. J.; Martin, R. L. Revised Basis Sets for the LANL Effective Core Potentials. *J. Chem. Theory Comput.* **2008**, *4*, 1029−1031. (d) Schaefer, A.; Horn, H.; Ahlrichs, R. Fully Optimized Contracted Gaussian-Basis Sets for Atoms Li to Kr. *J. Chem. Phys.* **1992**, *97*, 2571.

(17) Weigend, F.; Ahlrichs, R. Balanced Basis Sets of Split Valence, Triple Zeta Valence and Quadruple Zeta Valence Quality for H to Rn: Design and Assessment of Accuracy. *Phys. Chem. Chem. Phys.* **2005**, *7*, 3297−3305.

(18) Martin, R. L. Natural Transition Orbitals. *J. Chem. Phys.* **2003**, *118*, 4775−4777.

(19) (a) Shao, Y.; Mei, Y.; Sundholm, D.; Kaila, V. R. I. Benchmarking the Performance of Time-Dependent Density Functional Theory Methods on Biochromophores. *J. Chem. Theory Comput.* **2019**, *16*, 587−600. (b) Laurent, A. D.; Jacquemin, D. TD-DFT Benchmarks: A Review. *Int. J. Quantum Chem.* **2013**, *113*, 2019−2039. (c) Fehér, P. P.; Purgel, M.; Joó, F. Performance of Exchange−Correlation Functionals on Describing Ground State Geometries and Excitations of Alizarin Red S: Effect of Complexation and Degree of Deprotonation. *Comput. Theor. Chem.* **2014**, *1045*, 113−122.

(20) (a) Fang, C.; Durbeej, B. Calculation of Free-Energy Barriers with TD-DFT: A Case Study on Excited-State Proton Transfer in Indigo. *J. Phys. Chem. A* **2019**, *123*, 8485−8495. (b) Wang, J.; Liu, Q.; Yang, D. Theoretical Insights into Excited-State Hydrogen Bonding Effects and Intramolecular Proton Transfer (ESIPT) Mechanism for BTS System. *Sci. Rep.* **2020**, *10*, 5119. (c) Lewis, F. D.; Bassani, D. M.; Caldwell, R. A.; Unett, D. J. Singlet State Cis,Trans Photoisomerization and Intersystem Crossing of 1-Arylpropenes. *J. Am. Chem. Soc.* **1994**, *116*, 10477−10485.

(21) (a) Sasikumar, D.; John, A. T.; Sunny, J.; Hariharan, M. Access to the Triplet Excited States of Organic Chromophores. *Chem. Soc. Rev.* **2020**, *49*, 6122−6140. (b) Gorman, A. A.; Gould, I. R.; Hamblett, I. Lifetimes and Energies of the Relaxed Triplet States of Cyclopentadiene and Tetramethylbutadiene. A Pulse Radiolysis and Pulsed Laser Study. *J. Am. Chem. Soc.* **1981**, *103*, 4553−4558.

(22) To show that the reaction on the S1 surface requires thermal activation, the *ipso* addition step for the neutral **1a** molecule was calculated (Figure S12). It has a barrier of +18.7 kcal/mol, consistent with a thermally activated reaction.

(23) Liu, F.; Chen, Y.; Houk, K. N. Huisgen's 1,3-Dipolar Cycloadditions to Fulvenes Proceed via Ambimodal [6+4]/[4+2] Transition States. *Angew. Chem., Int. Ed.* **2020**, *59*, 12412−12416.

(24) The most favorable ether cleavage is provided by the TFA assisted pathway as shown in Figure 3 with 0.7 kcal/mol barrier between **III*** and **IV**. The analogous step shown in Figure 2 between **2** and **3** requires 10.2 kcal/mol additional energy.

(25) Cramer, C. *Essentials of Computational Chemistry,* 2nd ed; Wiley: Chichester, 2004.

(26) (a) Skoog, D. A.; Holler, F. J.; Stanley, R. C. *Principles of Instrumental Analysis*, 6th Edition, Thomson Brooks/Cole. 2007. (b)) Harris, D. C.; Bertolucci, M. D. *Symmetry and Spectroscopy, An Introduction to Vibrational and Electronic Spectroscopy*; Dover Publications, Inc.: New York, 1989.

(27) Although the TFA salt model shown in Figure 4 would yield lower barriers, the *ipso* addition can be used more generally for this reaction (e.g., also for molecules that do not require an external acid). Here, the point was to show a simple approach to assess the effect of structure modifications.